Spectral Analysis of Channel Noise in Nanoscale MOSFETS

Giorgio Casinovi
School of Electrical and Computer Engineering
Georgia Institute of Technology
Atlanta, GA 30332-0250

ABSTRACT

This paper describes an algorithm for numerical computation of the power spectral density (PSD) of channel noise in nanoscale MOSFETs. Noise generation phenomena inside the channel are modeled as random processes, represented by distributed sources that are added to the equations describing charge transport in the channel. The resulting set of differential equations is then solved using a frequency-domain simulation algorithm, yielding the total noise PSD at the device terminals. Comparisons between simulated and measured values of the noise PSD can then be used to test the validity of noise models for nanoscale MOSFETs. Simulation results obtained on a MOSFET under various DC bias conditions are presented.

Keywords: Device modeling; simulation; noise.

1 INTRODUCTION

Noise generation in semiconductor devices has been studied for over fifty years. The best known model of channel noise in MOSFETs is due to van der Ziel [1]. While this model is sufficiently accurate for long-channel devices, discrepancies with experimental data in submicron devices were already observed more than fifteen years ago [2]. In fact, the van der Ziel model underestimates the thermal noise generated in short-channel devices; the origin of this excess noise has been the object of intense investigation for several years.

Some researchers have tried to obtain more accurate models by resorting to approaches based on the so-called impedance field method [3], which leads to modeling the channel as a linear, one-dimensional transmission line in which noise generation phenomena are represented by Langevin sources distributed throughout the length of the channel [4], [5]. Because the line parameters vary along the channel, better accuracy can be obtained by dividing the channel into multiple segments, where each segment is modeled as a uniform transmission line [6].

Based on the results of simulations performed using the approaches described above, it has been suggested that the excess noise can be explained in terms of nonlocal effects on the carrier velocity that are captured only by higher-order transport models, such as the hydrodynamic model [6], [7].

Other researchers, however, have offered different explanations of the same phenomenon, based on effects such as carrier velocity saturation and carrier heating. In short channel devices, carrier velocity saturates near the drain end of the channel due to the presence of high lateral electrical fields [8], [9]. This affects the local value of the channel conductance, which is normally expressed as: $G = \mu(x)q$, where $\mu(x)$ is the carrier mobility and q is the inversion layer charge density. Since the values of the local noise sources that model thermal noise in the channel depend on G, variations in carrier mobility along the channel must be accounted for. Moreover, the assumption that thermal equilibrium exists in the channel is no longer necessarily valid in the presence of high electric fields [9]. In order to account for the deviation of carrier density from its equilibrium value, a field-dependent equivalent temperature is introduced. Since the exact relationship between the equivalent temperature and the electric field cannot be obtained analytically, empirical formulae expressing a linear [9] or quadratic [10], [11] dependence on the electric field are used instead. Several models explaining the excess channel noise as due to carrier velocity saturation and carrier heating have been published in the literature [9]–[12].

This paper describes an algorithm to compute the noise PSD at the drain and source terminals of a MOSFET from frequency-domain simulations of the ordinary or partial differential equations used to model the device's behavior (e.g. the drift-diffusion equations). Specifically, noise generation inside the device is modeled as a stationary random process, and a relationship between the PSD of the noise sources and that of the resulting noise voltages or currents at the device terminals is obtained by linearizing the charge transport equation around the bias point of the device. This makes it possible to simulate a variety of models for noise generation phenomena inside MOSFETS and to compare the simulation results with experimental measurements to verify the validity of those models. A detailed description of the algorithm is given in the next section, and simulation results are presented in Sec. 3.

2 NOISE SPECTRAL ANALYSIS

The cross-section of a MOSFET device is shown in Fig. 1. For the purpose of noise analysis, a very simple model for the channel charge will be used, as described by the equa-

This work was supported in part by the National Science Foundation under grant CCR-0306343.

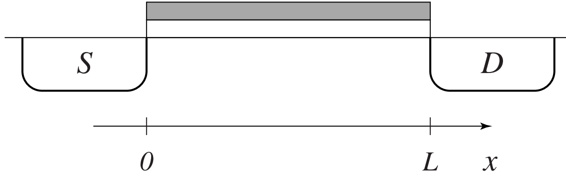

Figure 1: MOSFET cross-section

tion:

$$Q(x) = -C_{ox}[V(x) + V_t]$$

where Q is the charge in the channel, V the local voltage in the channel with respect to the *gate*, C_{ox} the gate oxide capacitance, and V_t the MOSFET threshold voltage. Based on this model, the voltage and current in the device channel must satisfy the following pair of partial differential equations:

$$\begin{aligned} \frac{\partial V}{\partial x} &= \frac{I}{\mu C_{ox}(V+V_t)} \\ \frac{\partial I}{\partial x} &= -C_{ox}\frac{\partial}{\partial t}(V+V_t) \end{aligned} \tag{1}$$

Noise generation mechanisms inside the channel can be modeled by the introduction of noise sources in the above equations:

$$\begin{aligned} \frac{\partial V}{\partial x} &= \frac{I}{\mu C_{ox}(V+V_t)} + v_n(x,t) \\ \frac{\partial I}{\partial x} &= -C_{ox}\frac{\partial}{\partial t}(V+V_t) + i_n(x,t) \end{aligned}$$

where $v_n(x,t)$ and $i_n(x,t)$ model noise generation phenomena inside the channel.

The noise sources cause perturbations v and i in the channel voltage and current, respectively. Assuming that those perturbations are small, they can be computed by linearizing the equations above around the DC solution:

$$\begin{aligned} \frac{\partial v}{\partial x} &= -\frac{I}{\mu C_{ox}(V+V_t)^2}v + \frac{1}{\mu C_{ox}(V+V_t)}i \\ &\quad + v_n(x,t) \\ \frac{\partial i}{\partial x} &= -C_{ox}\frac{\partial v}{\partial t} + i_n(x,t) \end{aligned} \tag{2}$$

This set of differential equations can be rewritten in matrix and vector notation as:

$$\frac{\partial \mathbf{f}}{\partial x} = \mathbf{G}(x)\mathbf{f} - \mathbf{C}\frac{\partial \mathbf{f}}{\partial t} + \mathbf{u}(x,t) \tag{3}$$

where: $\mathbf{f} = [\, v \; i \,]^T$ and

$$\begin{aligned} \mathbf{G}(x) &= \frac{1}{\mu C_{ox}}\begin{bmatrix} \frac{I}{[V(x)+V_t]^2} & \frac{-1}{[V(x)+V_t]} \\ 0 & 0 \end{bmatrix} \\ \mathbf{C} &= \begin{bmatrix} 0 & 0 \\ C_{ox} & 0 \end{bmatrix} \\ \mathbf{u}(x,t) &= \begin{bmatrix} v_n(x,t) \\ i_n(x,t) \end{bmatrix} \end{aligned}$$

Equation (3) can be discretized with respect to x by selecting points $x_0 = 0 < x_1 < \ldots < x_N = L$ and using an appropriate numerical integration algorithm, such as the trapezoidal method:

$$\begin{aligned} \mathbf{f}_{n+1} &= \mathbf{f}_n + \frac{h_n}{2}\Big[\mathbf{G}_{n+1}\mathbf{f}_{n+1} - \mathbf{C}\frac{d\mathbf{f}_{n+1}}{dt} \\ &\quad + \mathbf{u}_{n+1}(t) + \mathbf{G}_n\mathbf{f}_n - \mathbf{C}\frac{d\mathbf{f}_n}{dt} + \mathbf{u}_n(t)\Big] \end{aligned} \tag{4}$$

where $h_n = x_{n+1} - x_n$ and for the sake of brevity the following notation has been used:

$$\begin{aligned} \mathbf{f}_n &= \mathbf{f}(x_n, t) \\ \mathbf{G}_n &= \mathbf{G}(x_n) \\ \mathbf{u}_n(t) &= \mathbf{u}(x_n, t) \end{aligned}$$

Equation (4) can be rewritten as:

$$\begin{aligned} &\frac{h_n}{2}\mathbf{C}\frac{d\mathbf{f}_n}{dt} + \frac{h_n}{2}\mathbf{C}\frac{d\mathbf{f}_{n+1}}{dt} = (\mathbf{I} + \frac{h_n}{2}\mathbf{G}_n)\mathbf{f}_n \\ &\quad - (\mathbf{I} - \frac{h_n}{2}\mathbf{G}_{n+1})\mathbf{f}_{n+1} + \frac{h_n}{2}[\mathbf{u}_{n+1}(t) + \mathbf{u}_n(t)] \end{aligned}$$

This system of differential equations can be written in matrix form as:

$$\mathcal{C}\frac{d\mathbf{F}}{dt} + \mathcal{G}\mathbf{F} = \mathbf{U}(t) \tag{5}$$

where:

$$\mathbf{F} = \begin{bmatrix} \mathbf{f}_0 \\ \vdots \\ \mathbf{f}_N \end{bmatrix}, \; \mathbf{U}(t) = \begin{bmatrix} \frac{h_0}{2}[\mathbf{u}_0(t) + \mathbf{u}_1(t)] \\ \vdots \\ \frac{h_{N-1}}{2}[\mathbf{u}_{N-1}(t) + \mathbf{u}_N(t)] \end{bmatrix}$$

and block matrices $\mathcal{C}$ and $\mathcal{G}$ are shown in Fig. 2.

It will be assumed that $\mathbf{U}(t)$ is a realization of a zero-mean stationary stochastic process. Let $\mathbf{R}_U(t_1,t_2)$ be its autocorrelation function:

$$\mathbf{R}_U(t_1,t_2) = E\left\{\mathbf{U}(t_1)\mathbf{U}^T(t_2)\right\}$$

Since the process is stationary, $\mathbf{R}_U(t_1,t_2)$ depends only on $\tau = t_1 - t_2$: $\mathbf{R}_U(t_1,t_2) = \mathbf{R}_U(t_1 - t_2) = \mathbf{R}_U(\tau)$, and the process's PSD is given by the Fourier transform of $\mathbf{R}_U(\tau)$ [13]:

$$\mathbf{S}_U(j\omega) = \int_{-\infty}^{+\infty} \mathbf{R}_U(\tau)e^{-j\omega\tau}\, d\tau$$

The autocorrelation function of $\mathbf{F}(t)$ can be computed by multiplying (5) by its transposed and taking the expected value of both sides of the resulting equation:

$$\begin{aligned} &E\left\{[\mathcal{C}\dot{\mathbf{F}}(t_1) + \mathcal{G}\mathbf{F}(t_1)][\mathcal{C}\dot{\mathbf{F}}(t_2) + \mathcal{G}\mathbf{F}(t_2)]^T\right\} \\ &\quad = E\left\{\mathbf{U}(t_1)\mathbf{U}^T(t_2)\right\} \end{aligned} \tag{6}$$

$$
\mathcal{C} = \begin{bmatrix} h_0\mathbf{C}/2 & h_0\mathbf{C}/2 & & & \\ & h_1\mathbf{C}/2 & h_1\mathbf{C}/2 & & \\ & & \ddots & & \\ & & & h_N\mathbf{C}/2 & h_N\mathbf{C}/2 \end{bmatrix}
$$

$$
\mathcal{G} = \begin{bmatrix} -\mathbf{I} - h_0\mathbf{G}_0/2 & \mathbf{I} - h_0\mathbf{G}_1/2 & & & \\ & -\mathbf{I} - h_1\mathbf{G}_1/2 & \mathbf{I} - h_1\mathbf{G}_2/2 & & \\ & & \ddots & & \\ & & & -\mathbf{I} - h_N\mathbf{G}_{N-1}/2 & \mathbf{I} + h_N\mathbf{G}_N/2 \end{bmatrix}
$$

Figure 2: Block matrices $\mathcal{C}$ and $\mathcal{G}$

It can be shown [13] that:

$$
\begin{aligned}
E\left\{\dot{\mathbf{F}}(t_1)\mathbf{F}^T(t_2)\right\} &= \frac{\partial \mathbf{R}_F}{\partial t_1} \\
E\left\{\mathbf{F}(t_1)\dot{\mathbf{F}}^T(t_2)\right\} &= \frac{\partial \mathbf{R}_F}{\partial t_2} \\
E\left\{\dot{\mathbf{F}}(t_1)\dot{\mathbf{F}}^T(t_2)\right\} &= \frac{\partial^2 \mathbf{R}_F}{\partial t_1 \partial t_2}
\end{aligned}
$$

Therefore (6) can be rewritten as:

$$
\begin{aligned}
&\mathcal{C}\frac{\partial^2 \mathbf{R}_F}{\partial t_1 \partial t_2}\mathcal{C}^T + \mathcal{C}\frac{\partial \mathbf{R}_F}{\partial t_1}\mathcal{G}^T \\
&+ \mathcal{G}\frac{\partial \mathbf{R}_F}{\partial t_2}\mathcal{C}^T + \mathcal{G}\mathbf{R}_F\mathcal{G}^T = \mathbf{R}_U(t_1, t_2)
\end{aligned} \tag{7}
$$

Since $\mathbf{F}(t)$ is also a realization of a stationary process, its autocorrelation function depends only on $t_1 - t_2$: $\mathbf{R}_F(t_1, t_2) = \mathbf{R}_F(t_1 - t_2) = \mathbf{R}_F(\tau)$. Consequently:

$$
\begin{aligned}
\frac{\partial \mathbf{R}_F}{\partial t_1} &= \mathbf{R}'_F(\tau) \\
\frac{\partial \mathbf{R}_F}{\partial t_2} &= -\mathbf{R}'_F(\tau) \\
\frac{\partial^2 \mathbf{R}_F}{\partial t_1 \partial t_2} &= -\mathbf{R}''_F(\tau)
\end{aligned}
$$

Thus taking the Fourier transform of (7) yields:

$$
\begin{aligned}
&\omega^2\mathcal{C}\mathbf{S}_F(j\omega)\mathcal{C}^T + j\omega\mathcal{C}\mathbf{S}_F(j\omega)\mathcal{G}^T \\
&\quad - j\omega\mathcal{G}\mathbf{S}_F(j\omega)\mathcal{C}^T + \mathcal{G}\mathbf{S}_F(j\omega)\mathcal{G}^T = \mathbf{S}_U(j\omega)
\end{aligned}
$$

or equivalently:

$$
\mathcal{H}(j\omega)\mathbf{S}_F(j\omega)\mathcal{H}^*(j\omega) = \mathbf{S}_U(j\omega) \tag{8}
$$

where $\mathbf{S}_F(j\omega)$ is the PSD of $\mathbf{F}$, $\mathcal{H}(j\omega) = j\omega\mathcal{C} + \mathcal{G}$ and $\mathcal{H}^*$ denotes the adjoint (conjugate transposed) of $\mathcal{H}$.

This equation can be solved by performing an LU decomposition of $\mathcal{H}$: $\mathcal{H}(j\omega) = \mathcal{L}(j\omega)\mathcal{U}(j\omega)$. In principle, it is possible to solve for $\mathbf{S}_F(j\omega)$ directly:

$$
\begin{aligned}
&\mathbf{S}_F(j\omega) \\
&= \mathcal{U}^{-1}(j\omega)\mathcal{L}^{-1}(j\omega)\mathbf{S}_U(j\omega)[\mathcal{L}^*(j\omega)]^{-1}[\mathcal{U}^*(j\omega)]^{-1}
\end{aligned}
$$

Numerical round-off error introduced in the computation of $\mathbf{S}_U(j\omega)$, however, could yield a solution that is not a positive-definite self-adjoint matrix, a non-physical result. For this reason it is preferable to compute $\mathbf{S}_F(j\omega)$ in factored form through a Cholesky decomposition of $\mathbf{S}_U(j\omega)$:

$$
\begin{aligned}
\mathbf{S}_U(j\omega) &= \mathbf{L}_U(j\omega)\mathbf{L}_U^*(j\omega) \\
\mathbf{W}_F(j\omega) &= \mathcal{U}^{-1}(j\omega)\mathcal{L}^{-1}(j\omega)\mathbf{L}_U(j\omega) \\
\mathbf{S}_F(j\omega) &= \mathbf{W}_F(j\omega)\mathbf{W}_F^*(j\omega)
\end{aligned}
$$

This ensures that the resulting $\mathbf{S}_F(j\omega)$ is a positive-definite self-adjoint matrix.

3 NUMERICAL RESULTS

The algorithm described in the previous section was used to compute the noise PSD at the source and drain terminals of a MOSFET under various bias conditions. It was assumed that the noise sources represented by $i_n(x,t)$ and $v_n(x,t)$ in (2) where white, uniformly distributed in the device channel, and uncorrelated. Under these assumptions, $\mathbf{S}_U(j\omega)$ is block-diagonal and independent of ω. Figures 3 and 4 show the simulated noise PSD at the drain (solid line) and source (dashed line) ends of the MOSFET for two different values of V_{ds}.

This approach can be applied to more complex and accurate models of carrier transport and noise generation mechanisms inside the channel. For example, (1) can be replaced by the drift-diffusion equations:

$$
\begin{aligned}
\varepsilon\nabla^2 V &= -q(N_D - N_A + p - n) \\
\frac{1}{q}\nabla\cdot\mathbf{J}_n &= \frac{\partial n}{\partial t} - (G - R) \\
\frac{1}{q}\nabla\cdot\mathbf{J}_p &= -\frac{\partial p}{\partial t} + (G - R) \\
\mathbf{J}_n &= -q\mu_n n\nabla V + qD_n\nabla n \\
\mathbf{J}_p &= -q\mu_p p\nabla V - qD_p\nabla p
\end{aligned}
$$

If a one-dimensional model of the device is used, only one spatial variable is retained, and this set of partial differential equations can be discretized following the approach de-

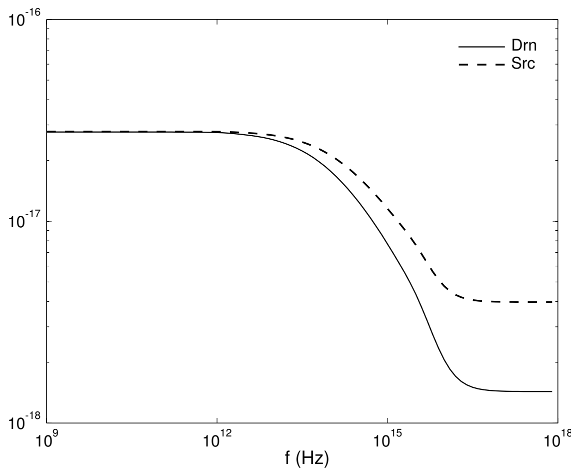

Figure 3: Noise power spectral density, $V_{ds} = 0.2\text{V}$

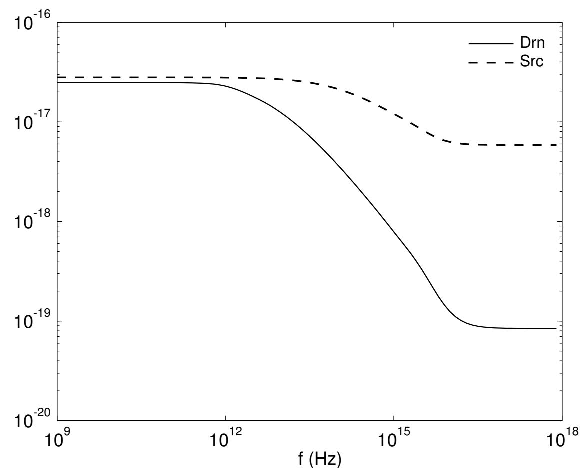

Figure 4: Noise power spectral density, $V_{ds} = 0.44\text{V}$

scribed in Section 2. For better accuracy, two- or three-dimensional device geometries can be used, in which case more complex discretization schemes become necessary.

Similarly, noise generation phenomena inside the device can be modeled more accurately. For example, experimental data and theoretical analysis indicate that the noise sources inside the device are not uncorrelated [14]. Correlation among noise sources can be accounted for by introducing off-diagonal terms in $\mathbf{S}_U(j\omega)$. Regardless of the complexity of the geometry of the device and of the models, computation the noise PSD at the device terminals can be performed following the approach described earlier. Comparisons of simulation results with experimental data, can provide information useful in developing noise models for nanoscale MOSFET devices.

REFERENCES

[1] A. van der Ziel, *Noise in Solid State Devices and Circuits*. New York, NY: Wiley, 1986.

[2] A. A. Abidi, "High-frequency noise measurements on FET's with small dimensions," *IEEE Trans. Electron Devices*, vol. ED-33, no. 11, pp. 1801–1805, November 1986.

[3] W. Shockley, J. A. Copeland, and R. P. James, "The impedance field method of noise calculation in active semiconductor devices," in *Quantum Theory of Atoms, Molecules, and the Solid State*, P. O. Lowdin, Ed. New York, NY: Academic Press, 1966, p. 537.

[4] A. Cappy and W. Heinrich, "High-frequency FET noise performance: A new approach," *IEEE Trans. Electron Devices*, vol. 36, no. 2, pp. 403–409, February 1989.

[5] F. Danneville, H. Happy, G. Dambrine, J.-M. Belquin, and A. Cappy, "Microscopic noise modeling and macroscopic noise models: How good a connection?" *IEEE Trans. Electron Devices*, vol. 41, no. 5, pp. 779–786, May 1994.

[6] J.-S. Goo, C.-H. Choi, F. Danneville, E. Morifuji, H. S. Momose, Z. Yu, H. Iwai, T. H. Lee, and R. W. Dutton, "An accurate and efficient high frequency noise simulation technique for deep submicron MOSFETs," *IEEE Trans. Electron Devices*, vol. 47, no. 12, pp. 2410–2419, December 2000.

[7] J.-S. Goo, C.-H. Choi, A. Abramo, J.-G. Ahn, Z. Yu, T. H. Lee, and R. W. Dutton, "Physical origin of the excess thermal noise in short channel MOSFETs," *IEEE Electron Dev. Lett.*, vol. 22, no. 2, pp. 101–103, February 2001.

[8] B. Wang, J. R. Hellums, and C. G. Sodini, "MOSFET thermal noise modeling for analog integrated circuits," *IEEE Jour. Solid-State Circuits*, vol. 29, no. 7, pp. 833–835, July 1994.

[9] P. Klein, "An analytical thermal noise model of deep submicron MOSFET's," *IEEE Electron Dev. Lett.*, vol. 20, no. 8, pp. 399–401, August 1999.

[10] D. P. Triantis, A. N. Birbas, and D. Kondis, "Thermal noise modeling for short-channel MOSFET's," *IEEE Trans. Electron Devices*, vol. 43, no. 11, pp. 1950–1955, November 1996.

[11] G. Knoblinger, P. Klein, and M. Tiebout, "A new model for thermal channel noise of deep submicron MOSFET'S and its application in RF-CMOS design," in *Proc. 2000 Symp. VLSI Circuits*, 2000, pp. 150–153.

[12] C. H. Chen and M. J. Deen, "High frequency noise of MOSFETs. I: Modeling," *Solid-State Electronics*, vol. 42, no. 11, pp. 2069–2081, November 1998.

[13] A. Papoulis, *Probability, Random Variables, and Stochastic Processes*. New York, NY: McGraw-Hill Book Co., 1965.

[14] J.-P. Nougier, "Fluctuations and noise of hot carriers in semiconductor materials and devices," *IEEE Trans. Electron Devices*, vol. 41, no. 11, pp. 2034–2049, Nov. 1994.